Mitosis of Hepatitis B virus-infected cells results in uninfected daughter cells

Thomas Tu (t.tu@sydney.edu.au)
Westmead Institute for Medical Research
Benno Zehnder
University Hospital Heidelberg https://orcid.org/0000-0002-4910-2636
Jochen Wettengel
Institute of Virology, School of Medicine, Technical University of Munich / Helmholtz Zentrum München
Henrik Zhang
The Westmead Institute for Medical Research
Sally Coulter
University of Sydney
Vikki Ho
Storr Liver Centre
Mark Douglas
https://orcid.org/0000-0003-4621-3485
Ulrike Protzer
School of Medicine, Technical University of Munich / Helmholtz Zentrum München
https://orcid.org/0000-0002-9421-1911
Jacob George
The Westmead Institute for Medical Research https://orcid.org/0000-0002-8421-5476
Stephan Urban
University Hospital Heidelberg

Article

Keywords: Covalently closed circular DNA, Hepatitis B virus, viral persistence, cinqPCR

Posted Date: February 9th, 2022

DOI: https://doi.org/10.21203/rs.3.rs-1325894/v1

Title: Mitosis of Hepatitis B virus-infected cells results in uninfected daughter cells

Authors:

Thomas Tu[1,2], Benno Zehnder[3], Jochen M. Wettengel[4], Henrik Zhang[1], Sally Coulter[1], Vikki Ho[1], Mark W. Douglas[1,2], Ulrike Protzer[4,5], Jacob George[1]*, Stephan Urban[3,6]*

Affiliations:

[1] Storr Liver Centre, Westmead Clinical School and Westmead Institute for Medical Research, Faculty of Medicine and Health, The University of Sydney, Westmead, NSW 2145, Australia

[2] Sydney Institute for Infectious Diseases, University of Sydney at Westmead Hospital, Westmead NSW 2145, Australia.

[3] Department of Infectious Diseases, Molecular Virology, University Hospital Heidelberg, Heidelberg, Germany

[4] Institute of Virology, Technische Universität München/Helmholtz Zentrum München, Munich, Germany.

[5] German Center for Infection Research (DZIF), Munich Partner Site, Munich, Germany

[6] German Center for Infection Research (DZIF), Heidelberg Partner Site, Heidelberg, Germany

Corresponding Author: Dr. Thomas Tu, t.tu@sydney.edu.au; thomas.tu.phd@gmail.com

Keywords: Covalently closed circular DNA, Hepatitis B virus, viral persistence, cinqPCR

Abstract

Chronic hepatitis B is a major cause of liver failure and liver cancer, resulting in 600,000 annual deaths globally. Infection chronicity (and resultant liver disease) is determined by intrahepatic persistence of the viral covalently closed circular DNA (cccDNA), an episomal form that encodes all viral transcripts. Therefore, cccDNA is a key target for new treatments, with the ultimate aim of its elimination. While established cccDNA molecules are stable in resting hepatocytes, their fate in dividing cells is not well understood. Using highly-sensitive quantification assays, we observed a dramatic reduction in cccDNA levels, HBV-positive cell numbers, and cccDNA-dependent protein expression after each round of cell mitosis. These observations are consistent with a complete loss (as opposed to a dilution) of cccDNA in daughter cells. Our results thus show that HBV persistence can be efficiently overcome by inducing cell mitosis and justify therapeutic approaches that induce liver turnover (e.g. immune modulators) as an adjunct to achieve Hepatitis B cure.

Introduction

Hepatitis B virus (HBV) is an enveloped, partially double-stranded DNA virus and the prototypic member of the *Hepadnaviridae*. Chronic infection with HBV confers a high risk of developing liver cirrhosis and hepatocellular carcinoma, causing ~600 000 deaths annually[1]. HBV is not cytopathic; instead, liver injury is driven by virus-induced inflammatory immune responses that are insufficient to eradicate infected hepatocytes. Thus, chronic HBV infection is often a life-long and incurable condition, which in turn drives other personal impacts (e.g. anxiety about disease progression, stigma and discrimination, and long-term health care costs)[2].

Persistence of covalently closed circular viral DNA (cccDNA) in the hepatocyte is the critical determinant of chronic hepatitis B infection. cccDNA is an episomal plasmid-like "mini-chromosome" that acts as the transcriptional template for HBV mRNAs and the pregenomic RNA and is therefore necessary for viral replication. However, the host immune responses are usually sub-optimal and cannot fully eliminate all cccDNA-containing hepatocytes. Given its supercoiled structure and complexing with cellular histones, cccDNA is stable within an infected hepatocyte (likely for its entire lifetime) [3,4], though some studies have suggested partial non-cytolytic clearance[5-7]. Additional routes of cccDNA elimination from the liver are immune-mediated killing of cccDNA-containing hepatocytes and possibly loss following mitosis[8]. Understanding the mechanisms behind the elimination of cccDNA will greatly aid in developing therapeutics to overcome chronic HBV infections.

Elimination of cccDNA in infected hepatocytes would result in a cure of chronic HBV[9], which cannot be efficiently achieved by current treatment options. Clearance of cccDNA would allow cessation of therapy without viral rebound, thereby slowing liver pathogenesis. Mathematical models predict that various independent parameters (including the cccDNA copy number per cell, its rate of degradation, and its stability in resting and replicating cells) profoundly affect the dynamics of cccDNA clearance[10,11]. These dynamics are not fully resolved as there is controversy as to whether

mitosis of an infected cell results in two uninfected daughter cells[8,12] or if cccDNA survives and is diluted amongst the daughter cells[4,10,13,14].

The reduction of cccDNA levels with mitosis critically determines the optimal cure strategy: for example, if the cccDNA pool of an infected hepatocyte is lost within one round of mitosis, then activation of antiviral immunity or other methods to induce turnover of infected cells become an attractive option for treatment. On the other hand, if cccDNA survives mitosis greater emphasis on cccDNA degrading pathways (e.g. CRISPR-Cas9) or direct killing of infected cells (e.g. CAR-T cell technology) may be of higher priority. Given the central importance of cccDNA reduction for how the field should proceed with therapeutic cures of chronic hepatitis B, we aimed to clarify the fate of cccDNA after cell mitosis.

We used a novel **c**ccDNA **in**version **q**uantitative (cinq)PCR assay[15,16] to precisely quantify cccDNA levels. We find that cccDNA levels undergo a ~5-fold decrease after each round of mitosis, which is the exact rate predicted by mathematical models assuming a complete loss of cccDNA in daughter cells. Evidence from orthogonal approaches using reporter HBV viruses was consistent with this model, down to the level of a single cell. Thus, we unequivocally show that liver turnover is an efficient mechanism to clear HBV cccDNA, which informs future therapeutic approaches to the cure of chronic hepatitis B.

Results

Prediction of cccDNA levels following mitosis

We predicted the levels of cccDNA following cell mitosis given each of the two major hypothetical models: i) the **cccDNA loss** model, where the cccDNA pool in an infected cell is not conveyed at all to the daughter cells after mitosis; and ii) the **cccDNA dilution** model, where the entire cccDNA pool is distributed amongst the daughter cells.

We assumed that each cell has an equal probability of undergoing mitosis, thereby resulting in a Poisson frequency distribution in rounds of mitosis per cell. This assumption predicts that 63.2% of cells would undergo at least one mitosis cycle following an average of one cell division of the bulk population. Thus, in the model where cccDNA is completely lost after mitosis, 36.8% of cells maintain their cccDNA. Assuming cccDNA is diluted upon mitosis and no new cccDNA is formed[16], the cccDNA copy numbers do not change.

In both the loss and dilution models, the cell population doubles; thus the number of cccDNA molecules per cell reduces by 50%. Thus, the loss model predicts an average net reduction to 18.4% of initial cccDNA levels per cell after each round of mitosis, whereas the dilution model predicts a reduction to 50% per round of mitosis. In both models, this predicted reduction is independent of the size of the cccDNA pool per individual cell.

HBV cccDNA levels profoundly decline following cell division, indicating complete elimination in daughter cells

We tested these predictions in two different HBV-susceptible cell lines, HepG2-NTCP and HepaRG-NTCP cells. After initial cccDNA establishment (3 days post-infection, dpi), the infected cells were serially passaged (1:2) every 3 days to induce cell mitosis. We developed two experimental setups

(Figure 1A): Setup 1, where total cellular DNA was extracted immediately following the splitting procedure; and Setup 2, where cells were cultured until 12 dpi to control for any cccDNA level changes occurring during the time course (e.g. via cccDNA amplification or degradation in resting cells). cccDNA molecules per cell were then precisely quantified by cinqPCR. Decreases in cccDNA levels following splitting closely matched those expected from the loss model in both HepG2-NTCP (Figure 1B) and HepaRG-NTCP (Figure 1C) cells.

Abrogation of HBV replication did not increase rates of cccDNA loss

In the previous experiment, we had not blocked viral replication. We tested if the mitosis-dependent reduction in cccDNA levels could be accelerated by inhibiting viral replication, as cccDNA has been assumed to be replenished by nuclear import of mature nucleocapsids in the cytosol. Such a mechanism can be impeded using a replication-deficient virus. Therefore, we investigated the post-mitotic levels of cccDNA in HepG2-NTCP cells infected with replication-deficient HBV with an early stop codon in the HBV core protein (HBc) open reading frame[16]. If the nuclear import pathway was indeed active, then cccDNA levels would be lower in cells infected with HBc-deficient mutants compared to wild-type HBV. This experimental setup also tests the contribution of *de novo* HBV spread in the culture to cccDNA levels (though this is not expected to occur in cell culture as shown previously[16]).

We observed no difference in the rate of cccDNA reduction during serial rounds of mitosis between cells infected with HBc-deficient HBV or wild-type virus in Setups 1 or 2, as described in Figure 1 (Figure 2). We conclude that HBV spread, replication, or cytoplasmic mature nucleocapsids do not play significant roles in cccDNA levels after mitosis of HBV-infected daughter cells. Moreover, this information allows us to use replication-defective reporter virus to further investigate cccDNA loss, knowing that the lack of virus replication would not impact these dynamics.

Expression from cccDNA declines at a rate consistent with cccDNA loss with mitosis

We determined if protein expression from cccDNA also declined at the same rate as cccDNA copy number. We found that the detection of secreted viral antigens (HBeAg and HBsAg) by ELISA was insufficiently sensitive to precisely and accurately determine the relatively low levels of secretion after several rounds of mitosis (data not shown). We instead used a reporter HBV encoding secreted Gaussia Luciferase under a transcriptionally-strong TTR-promoter (rHBV-TTR-GLuc) in place of the HBsAg open reading frame (ORF) to infect HepG2-NTCP cells and used a serial-splitting experimental design similar to setup 2 described above (Figure 3A). Luciferase activity can be detected with much higher sensitivity compared to HBV antigens and was measured in the supernatant of infected cells 6 days following passage (thereby allowing cells to divide and then secrete sufficient luciferase into the supernatant).

Reduction of luciferase activity paralleled the reduction of cccDNA levels expected by the loss model (i.e. a reduction of ~5-fold with each successive split) compared to the dilution model (2-fold reduction per split), except for cells after the third passage where high variation (due to low signal) prevented clear observation of signal reduction. Luciferase activity was relatively stable after reaching a plateau, suggesting there were no fluctuations due to temporary epigenetic changes of transgene expression after cellular mitosis. Luciferase activity of negative controls pre-treated with virus entry inhibitor Myrcludex B never exceeded 0.8% at any time point, indicating that all detected signals were due to *bona fide* HBV infection. In conclusion, we show that the HBV cccDNA that is lost with mitosis is transcriptionally-active and its loss parallels the reduction in viral protein expression.

HBV-positive cells were rarely clustered after mitosis and decreased at rates consistent with complete cccDNA loss

We next visualised HBV-infected cells from Setup 2 on a single-cell level using immunofluorescence for HBc. HepG2-NTCPs showed a marked reduction in HBc-positive cell numbers after cell mitosis

(Figure 4A). The HBc-positive cells after mitosis induction present as individual cells (likely infected cells that have not undergone mitosis), which is consistent with the loss model. On the contrary, the dilution model would predict some cluster formation of two or more adjacent HBc-positive cells. Identical patterns were seen in HepaRG-NTCP cells (Figure S1). The number of HBc-positive cells (Figure 4B) at each passage more closely matched mathematical models where 2 HBc-negative daughter cells result from mitosis (complete loss), compared to those where either 1 or 2 HBc-positive daughter cells results from mitosis of infected cells (dilution model). Together, these data provide further support for the complete loss model.

Live cell imaging showed daughter cells of HBV-infected hepatocytes are viable and express no new viral antigens after mitosis

Finally, we determined the fate of individual HBV-infected cells that undergo mitosis; specifically, whether they undergo cell death or if they do indeed produce two uninfected daughter cells. To track living HBV-infected cells, we infected HepG2-NTCP cells with a reporter HBV that expresses turboRFP under the control of a TTR-promoter (rHBV-TTR-tRFP) (hereafter referred to as "tRFP-HBV"). Given the long half-life of tRFP mRNA (~10hrs[17]) and protein (~40 hours[18]), we were able to track the mitosis of cells expressing cccDNA-encoded proteins and the daughter cells by live imaging.

HepG2-NTCP cells infected with tRFP-HBV were seeded in DMSO-free DMEM into chamber slides at ~100,000 cells per cm^2 (about the concentration of a 1:1.5 split in comparison to previous experiments) allowing us to observe areas of high confluence (and therefore low mitosis) as well as low confluence/high mitosis. Live cell imaging was carried out over 36 hours. In areas of low confluence, we observed multiple instances of tRFP-positive cells undergoing mitosis, producing 2 living daughter cells containing tRFP. In high confluence areas, tRFP expression was stable in non-dividing cells. Thus, division of HBV-infected cells does not induce cell death of daughter cells.

We then tested if new tRFP was being expressed in the daughter cells by photo-bleaching all existing tRFP. After exposure to 560/40nm light for 10 minutes, cells were allowed to recover for 5 hours and reimaged. All tRFP-positive cells that had undergone mitosis in low confluence areas had lost positive signals, whereas the cells that did not undergo mitosis (in high confluence areas and the rare cells in low confluence areas) maintained positivity for tRFP. This suggests that HBV-infected cells lose cccDNA directly after mitosis.

Discussion

In this study, we provide mathematical modelling and multiple lines of evidence unequivocally showing that cccDNA is not propagated to daughter cells after mitosis. Reduction of cccDNA levels in HepG2-NTCP (a hepatoma cell line) and HepaRG-NTCP (a hepatocyte-like cell line differentiated from bipotent progenitor cells) suggests that cccDNA is lost after mitosis of an infected cell. Thus, this non-cytolytic pathway for cccDNA clearance via cell mitosis is highly efficient.

Some reports have suggested partial maintenance of cccDNA molecules in daughter cells after mitosis[4,10,13,14]. These studies have generally used non-human model systems in which higher numbers of cccDNA per cell are generated: these include woodchuck[4] and duck[10] models, and HepAD38 cells[13] in which viral replication and subsequent cccDNA formation is controlled by tetracycline. Moreover, nuclear import of mature nucleocapsids is a highly active feature in animal and over-expression models, but this route appears to contribute minimally to the cccDNA levels in human HBV infection models *in vitro*[16]. Future work is needed to confirm that these dynamics extend to the HBV-infected liver in humans.

Another difference to previous studies is the extent of mitosis induced: our experiments focused on only a few rounds of mitosis, whereas others performed splitting at higher dilutions and measured over longer periods – up to 30 weeks – after infection. For example, a previous report studied immune deficient uPA/SCID/beige mice implanted with HBV-infected hepatocytes, which repopulate the mouse liver after multiple rounds of mitosis[8]. In this system and consistent with the present data, rare non-dividing cells were found to maintain infection, while virus was eliminated in the bulk repopulated culture.

This data suggests heterogeneity in the host-cell population, where slow-growing or non-dividing cells may effectively act as viral reservoirs (consistent with previously published mathematical

models[19]). In agreement with this hypothesis, previous studies show non-random hepatocyte repopulation with selective clonal expansion being observed in people with chronic hepatitis B and in animal models of hepatitis B[20-24] and other liver injuries[25]. The effect of these heterogeneous cellular behaviours suggests that deciphering which route plays the major role for cccDNA persistence may identify a more efficient mechanism to clear cccDNA.

The results described here also impact the interpretation of future studies of cccDNA decay and therapeutic reduction. For example, our work suggests that a 2-fold reduction in cccDNA per cell would result from a cumulative turnover of ~35% of the cells in a culture. Thus, even slight levels of cytotoxicity or cell mitosis (particularly over long periods of culture) could dramatically reduce cccDNA levels. We therefore recommend that studies of investigational drugs or therapeutic approaches to specifically reduce cccDNA should determine carefully if the induction of mitosis contributes to the mechanism of action.

On the other hand, our work justifies a focus on therapeutic approaches that induce liver turnover to efficiently clear high levels of cccDNA. Potential strategies include immuno-modulators to induce liver turnover, though these would require considered application to avoid hepatic decompensation or carcinogenic risk. A targeted agent that induces the mitosis of specifically HBV-infected cells could overcome these risks. This theoretical agent would be a part of a combination of therapies to effect a cure: new infection events need to be inhibited to prevent *de novo* cccDNA formation, which can be achieved by concomitant treatment with viral entry inhibitors, capsid inhibitors, and/or nucleot(s)ide analogues.

In summary, we have uncovered a fundamental aspect of cccDNA dynamics that impacts the understanding of the viral persistence driving chronic HBV infections. Given the strong evidence that mitosis of infected hepatocytes results in uninfected daughter cells, greater focus should be applied

241 to determine exactly how cccDNA can persist despite marked liver turnover during hepatic
242 inflammatory flares. The answer to this ongoing problem may hold the key to inducing a complete
243 cure of chronic hepatitis B.

Materials and methods

Production of HBV inoculums

For wild-type HBV, virus stocks were purified from the supernatant of HepAD38 cells by heparin affinity chromatography, as previously described[26,27]. For HBc-deficient HBV (and associated WT control), virus was further concentrated using a 100-kDa Amicon Ultra-15 centrifugal filter (UFC910024, Merck) from the supernatant of Huh7 cells transfected with plasmid constructs containing an over-length HBV genome (coding for HBV pgRNA and HBV proteins) and a complementing HBc overexpression plasmid (encoding HBc under a CMV promoter), as previously described[16].

Reporter viruses rHBV-TTR-GLuc and rHBV-TTR-tRFP were generated in HepG2 cell lines that were stably co-transduced with a plasmid expressing HBV Polymerase, Surface Proteins and X and a recombinant HBV genome construct encoding HBV pgRNA with the HBsAg ORF replaced by an ORF encoding either turbo-RFP or Gaussia luciferase under a TTR promoter (as previously described[28]). Reporter virus stocks were purified by heparin affinity chromatography and sucrose gradient ultracentrifugation of the supernatant of these cells, as previously described[29].

Cell culture and HBV infection

HepaRG-NTCP (differentiated as previously described[30]), and HepG2-NTCP cells[31] were used for *in vitro* infection. HepaRG-NTCP cells were cultivated in William's E media supplemented with 1.5% DMSO[32,33]. HepG2-NTCP cells were maintained in DMSO-free Dulbecco's Modified Eagle's Medium[31]. HepG2-NTCP or dHepaRG-NTCP cells were seeded in 12-well plates and infected with HBV at up to 500 VGE/cell in 250µL of culture media supplemented with 4% v/v polyethylene glycol 8000 (Sigma Aldrich, St. Louis, MO USA) and 1.5% v/v (for HepaRG-NTCP) or 2.5% v/v DMSO (for HepG2-NTCP). Cells were washed twice with 1x phosphate-buffered saline (PBS) at 24 hours post-infection. At 3, 6,

9, and 12dpi, cells were trypsinised and the cell suspension split in half; one half re-seeded in a new 12-well plate, and the other frozen at -20°C for DNA extraction and cinqPCR analysis. In an alternate experimental setup (setup 2), instead of harvesting the second half of the cell suspension for DNA extraction, they were re-seeded in a new 12-well plate but did not undergo further splitting and all cells were harvested at 12dpi.

Detection of HBc-positive cells by immunofluorescence

Cells were seeded onto 13mm diameter glass coverslips in 24-well plates. At cell harvest, culture media was aspirated from the cells, which were then washed with 1mL 1xPBS and fixed with 300µL 4% w/v formaldehyde for 20 minutes at room temperature. Cells were permeabilised with 0.25% v/v Triton-X in 1xPBS for 20 minutes at room temperature. HBV core antigen was then detected using a 1:3000 dilution of polyclonal rabbit anti-HBc antibody (B0586, Dako, Denmark)[33] overnight at 4°C. After washing with 1xPBS, 1:500 AF545-conjugated goat anti-rabbit secondary antibody (A-11010, Invitrogen) and 2µg/mL Hoechst 33342 (H1399, Invitrogen) in 1mL PBS was overlaid on the cells, which were incubated in the dark at room temperature for 1hr. Fluorescence microscopy images were taken at 40x magnification with appropriate DAPI and Texas Red filter sets. For each sample, an area the size of 5 random fields of view were acquired by NIS Elements Advanced software (Nikon, Minato, Tokyo, Japan). Images were edited with ImageJ imaging software[34] and quantified using Ilastik image classification, segmentation and analysis software (https://www.ilastik.org/, Version 1.3.3)[35].

Quantification of total HBV DNA, cccDNA, and cellular genome copy numbers by cinqPCR

The cinqPCR protocol was carried out as previously described[15,16,36]. Total cellular DNA was extracted from harvested cells using a NucleoSpin® Tissue kit (740952, Macherey-Nagel, Düren, Germany) as per the manufacturer's instructions and eluted in 50 µL of elution buffer. Ten µL of the DNA extract was digested in a 20 µL restriction digestion reaction containing 1x CutSmart buffer (B7204, New

England Biolabs, Ipswich, MA USA), 7.5U $RecJ_f$ (M0264, NEB), and 10 U *Hha*I (R0139, NEB). The combined restriction digestion and exonuclease reaction was incubated for 4 rounds of a 15 min interval at 37°C followed by a 15 min interval at 42°C. The enzymes were then heat-inactivated at 80°C for 20 min. To circularise the digested fragments, a 10 µL solution containing 500 U of T4 DNA Ligase (M0202, NEB) in 1x CutSmart buffer and 3 mMol molecular-grade ATP (P0756, NEB) was added to the reaction. The reaction was incubated at 16°C for 2 hr, followed by an inactivation step of 80°C for 20 min, and holding at 4°C. A final linearization step was performed by adding 5 µL solution containing 10 U *Xba*I (R0145, NEB) in 1x CutSmart buffer and incubating at 37°C for 2 hr, 80°C for 20 min, and then storing at 4°C until further use.

For digital droplet (dd)PCR analysis, 2 µL of the inverted product was put in a 20 µL ddPCR reaction composed of 1x ddPCR Supermix for Probes (1863024, Biorad, Hercules, CA USA), 1x VIC-labelled TaqMan™ Copy Number Reference Assay for the human RNase P gene (4403328, Applied Biosystems, Foster City, CA USA), and 150 pMol of each HBV DNA-specific primer and probe (all synthesized by Eurofins Scientific, Luxembourg). The forward, reverse and probe sequences for the inverted HBV cccDNA fragment were 5'-CACTCTATGGAAGGCGGGTA-3', 5'-ATAAGGGTCGATGTCCATGC-3', and 5'-FAM-AACACATAGCGCACCAGCA-BHQ1-3', respectively. The forward, reverse and probe sequences to detect total HBV DNA copies were 5'-GTGTCTGCGGCGTTTTATCA-3', 5'- GACAAACGGGCAACATACCTT-3', and 5'-FAM-TGAGGCATAGCAGCAGGATG-BHQ1-3', respectively. Droplets were generated according to the manufacturer's protocol using a QX200 Droplet Generator (Biorad). Intra-droplet PCR was carried out using the following protocol: an initial 10min denaturation, enzyme activation and droplet stabilization step at 95°C; followed by 40 cycles of a 10s denaturation step at 95°C, a 15s annealing step at 54°C and a 20s elongation step at 68°C, finished with a 10 minute enzyme deactivation step at 95°C. Products were then stored at 12°C until droplet reading using a QX200 Droplet Reader (Biorad), quantification using FAM and VIC channels, and data analysis using QuantaSoft (Biorad).

Quantifying cccDNA-dependent protein expression by measuring luciferase activity

HepG2-NTCP cells infected with ~500 VGE/cell of rHBV-TTR-GLuc in 24-well plates and serially split as per the experimental outline (Figure 3a). Supernatant was collected every 3 days, centrifuged at 500xg to remove cell debris, and then stored at -20°C. Pierce™ Gaussia Luciferase Flash Assay Kit (16158, ThermoFisher Scientific) was used to measure luciferase activity, per the manufacturer's instructions. In brief, 10µL of cell supernatant was added to a black opaque 96-well plate (6005270, Perkin Elmer, Waltham, MA, USA). 50µL of working solution (1X Coelenterazine in Gaussia Flash Assay Buffer) was added and mixed with a pipette. Luminescence was then immediately read with a SpectraMax iD5 Plate Reader (Molecular Devices, San Jose, CA, USA).

Detection of HBc-positive cells by live imaging microscopy

HepG2-NTCP cells infected as described above with ~500 VGE/cell of tRFP-HBV in a 24-well plate. At 3 days post-infection, cells were seeded into Nunc Lab-Tek™ 8-well chamber (ThermoFisher Scientific, 177402PK) slides at a concentration of ~100,000 cells per cm^2 in 400 µL DMSO-free DMEM to stimulate cell mitosis. After allowing cells to attach for 8 hours post-seeding, sliders were transferred into a humidity-, heat- and CO_2-controlled chamber connected to a Zeiss AxioVert 200M (Carl Zeiss Microscopy GmbH, Jena, Germany). RFP-positive cells were then visualised by phase microscopy and fluorescence using a Texas Red filter set (excitation: 560/40nm; emission: 630/75nm) with a 40x objective lens. Images were acquired every 15 min from 10 fields of view per slide for 36 hours. Each field of view was then exposed for a total of 10 minutes of 560/40nm light. After a recovery period of 4 hours, images from the same fields of view were then acquired exactly as described above with identical settings. Images were acquired by Zeiss Zen Pro imaging software (Carl Zeiss Microscopy GmbH) and edited with ImageJ imaging software[34].

Funding statement

This work received funding from: the German Centre for Infection Research (DZIF) TTU Hepatitis Projects 5.807 and 5.704 (T.T. and S.U.); the Deutsche Forschungsgemeinschaft (DFG, German Research Foundation) – Project number 240245660; SFB 1129 (B.Z. and S.U.) and – Project number 272983813 – TRR179 (TP 15) (S.U.); the Australian Centre for HIV and Hepatitis Virology Research (T.T.); and the Australian National Health and Medical Research Council Ideas Grant APP2002565 (T.T. and M.D.), Program Grants APP1053206, APP1149976 and Project grants APP1107178 and APP1108422 (J.G.); and the Robert W. Storr Bequest to the Sydney Medical Foundation (J.G.). Microscopy was performed at the Westmead Scientific Platforms, which are supported by the Westmead Research Hub, the Cancer Institute New South Wales, the National Health and Medical Research Council, and the Ian Potter Foundation.

Acknowledgements

We acknowledge: Drs. Yi Ni and Florian A. Lempp for reagents (cell lines and HBV inoculum); and Lisa Walter, Anja Rippert, Franziska Schlund, Dr. Christa Kuhn, and Westmead Research Hub for their technical assistance. We are grateful to Dr. Zhenfeng Zhang for helpful discussions, Miriam Kleinig for proofreading and Prof. Dr. Ralf Bartenschlager for continuous support.

Data availability statement

All data generated or analysed during this study are included in this published article (and its supplementary information files).

Competing interests

Stephan Urban is co-applicant and co-inventor on patents protecting HBV preS-derived lipopeptides (Myrcludex B) for the use of HBV/HDV entry inhibitors. Ulrike Protzer a co-founder and shareholder of SCG Cell Therapy. The other authors in this study declare no relevant competing interests.

Author contributions

T.T. conceived the concept of the project, designed and carried out the experiments, analyzed the data, generated figures and wrote the manuscript; B.Z. designed and carried out the HBc-deficient mutant experiments and assisted in writing the manuscript; H.Z., S.C., and V.H. assisted in the experimental design of, carried out experiments, and assisted in writing the manuscript; J.W. generated the reporter viruses, assisted in experimental design and contributed to writing the manuscript; U.P. provided funding for J.W. and assisted in writing the manuscript; M.D. and J.G. provided funding for T.T., V.H., and parts of the project, and contributed to writing the manuscript; S.U. provided funding for T.T. and B.Z. and parts of the project, contributed intellectual input on experimental design, and contributed to writing the manuscript.

References

1 Stanaway, J. D. *et al.* The global burden of viral hepatitis from 1990 to 2013: findings from the Global Burden of Disease Study 2013. *Lancet* **388**, 1081-1088, doi:10.1016/S0140-6736(16)30579-7 (2016).

2 Tu, T., Block, J. M., Wang, S., Cohen, C. & Douglas, M. W. The lived experience of chronic hepatitis B: a broader view of its impacts and why we need a cure. *Viruses* **12**, 515 (2020).

3 Moraleda, G. *et al.* Lack of effect of antiviral therapy in nondividing hepatocyte cultures on the closed circular DNA of woodchuck hepatitis virus. *J Virol* **71**, 9392-9399 (1997).

4 Dandri, M., Burda, M. R., Will, H. & Petersen, J. Increased hepatocyte turnover and inhibition of woodchuck hepatitis B virus replication by adefovir in vitro do not lead to reduction of the closed circular DNA. *Hepatology* **32**, 139-146, doi:10.1053/jhep.2000.8701 (2000).

5 Lucifora, J. *et al.* Specific and nonhepatotoxic degradation of nuclear hepatitis B virus cccDNA. *Science* **343**, 1221-1228, doi:10.1126/science.1243462 (2014).

6 Guidotti, L. G. *et al.* Viral clearance without destruction of infected cells during acute HBV infection. *Science* **284**, 825-829 (1999).

7 Murray, J. M., Wieland, S. F., Purcell, R. H. & Chisari, F. V. Dynamics of hepatitis B virus clearance in chimpanzees. *Proc Natl Acad Sci U S A* **102**, 17780-17785 (2005).

8 Allweiss, L. *et al.* Proliferation of primary human hepatocytes and prevention of hepatitis B virus reinfection efficiently deplete nuclear cccDNA in vivo. *Gut* **67**, 542-552, doi:10.1136/gutjnl-2016-312162 (2018).

9 Lok, A. S., Zoulim, F., Dusheiko, G. & Ghany, M. G. Hepatitis B cure: From discovery to regulatory approval. *J Hepatol* **67**, 847-861, doi:10.1016/j.jhep.2017.05.008 (2017).

10 Reaiche-Miller, G. Y. *et al.* Duck hepatitis B virus covalently closed circular DNA appears to survive hepatocyte mitosis in the growing liver. *Virology* **446**, 357-364, doi:10.1016/j.virol.2013.08.014 (2013).

11 Murray, J. M. & Goyal, A. In silico single cell dynamics of hepatitis B virus infection and clearance. *J Theor Biol* **366**, 91-102, doi:10.1016/j.jtbi.2014.11.020 (2015).

12 Lutgehetmann, M. *et al.* In vivo proliferation of hepadnavirus-infected hepatocytes induces loss of covalently closed circular DNA in mice. *Hepatology* **52**, 16-24, doi:10.1002/hep.23611 (2010).

13 Li, M., Sohn, J. A. & Seeger, C. Distribution of Hepatitis B Virus Nuclear DNA. *J Virol* **92**, doi:10.1128/JVI.01391-17 (2018).

14 Zhu, Y. *et al.* Kinetics of hepadnavirus loss from the liver during inhibition of viral DNA synthesis. *J Virol* **75**, 311-322 (2001).

15 Tu, T. *et al.* A novel method to precisely quantify Hepatitis B Virus covalently closed circular (ccc)DNA formation and maintenance. *Antiviral Res*, 104865, doi:10.1016/j.antiviral.2020.104865 (2020).

16 Tu, T., Zehnder, B., Qu, B. & Urban, S. De novo synthesis of Hepatitis B virus nucleocapsids is dispensable for the maintenance and transcriptional regulation of cccDNA *JHEP Reports*, doi:10.1016/j.jhepr.2020.100195 (2020).

17 Yang, E. *et al.* Decay rates of human mRNAs: correlation with functional characteristics and sequence attributes. *Genome Res* **13**, 1863-1872, doi:10.1101/gr.1272403 (2003).

18 Shaner, N. C. *et al.* Improving the photostability of bright monomeric orange and red fluorescent proteins. *Nat Methods* **5**, 545-551, doi:10.1038/nmeth.1209 (2008).

19 Lythgoe, K. A., Lumley, S. F., Pellis, L., McKeating, J. A. & Matthews, P. C. Estimating hepatitis B virus cccDNA persistence in chronic infection. *Virus Evol* **7**, veaa063, doi:10.1093/ve/veaa063 (2021).

20 Mason, W. S. *et al.* HBV DNA Integration and Clonal Hepatocyte Expansion in Chronic Hepatitis B Patients Considered Immune Tolerant. *Gastroenterology* **151**, 986-998 e984, doi:10.1053/j.gastro.2016.07.012 (2016).

21 Mason, W. S., Jilbert, A. R. & Summers, J. Clonal expansion of hepatocytes during chronic woodchuck hepatitis virus infection. *Proc Natl Acad Sci U S A* **102**, 1139-1144, doi:0409332102 [pii] 10.1073/pnas.0409332102 (2005).

22 Mason, W. S., Liu, C., Aldrich, C. E., Litwin, S. & Yeh, M. M. Clonal expansion of normal-appearing human hepatocytes during chronic hepatitis B virus infection. *J Virol* **84**, 8308-8315, doi:10.1128/JVI.00833-10 (2010).

23 Mason, W. S. *et al.* Detection of clonally expanded hepatocytes in chimpanzees with chronic hepatitis B virus infection. *J Virol* **83**, 8396-8408, doi:JVI.00700-09 [pii] 10.1128/JVI.00700-09 (2009).

24 Tu, T. *et al.* Clonal expansion of hepatocytes with a selective advantage occurs during all stages of chronic hepatitis B virus infection. *J Viral Hepat* **22**, 737-753, doi:10.1111/jvh.12380 (2015).

25 Wei, Y. *et al.* Liver homeostasis is maintained by midlobular zone 2 hepatocytes. *Science* **371**, doi:10.1126/science.abb1625 (2021).

26 Ladner, S. K. *et al.* Inducible expression of human hepatitis B virus (HBV) in stably transfected hepatoblastoma cells: a novel system for screening potential inhibitors of HBV replication. *Antimicrob Agents Chemother* **41**, 1715-1720, doi:10.1128/AAC.41.8.1715 (1997).

27 Lempp, F. A. *et al.* Evidence that hepatitis B virus replication in mouse cells is limited by the lack of a host cell dependency factor. *J Hepatol* **64**, 556-564, doi:10.1016/j.jhep.2015.10.030 (2016).

28 Wing, P. A. *et al.* A dual role for SAMHD1 in regulating HBV cccDNA and RT-dependent particle genesis. *Life Sci Alliance* **2**, doi:10.26508/lsa.201900355 (2019).

29 Wettengel, J. M. *et al.* Rapid and Robust Continuous Purification of High-Titer Hepatitis B Virus for In Vitro and In Vivo Applications. *Viruses* **13**, doi:10.3390/v13081503 (2021).

30 Gripon, P. *et al.* Infection of a human hepatoma cell line by hepatitis B virus. *Proc Natl Acad Sci U S A* **99**, 15655-15660, doi:10.1073/pnas.232137699 (2002).

31 Ni, Y. *et al.* Hepatitis B and D viruses exploit sodium taurocholate co-transporting polypeptide for species-specific entry into hepatocytes. *Gastroenterology* **146**, 1070-1083, doi:10.1053/j.gastro.2013.12.024 (2014).

32 Gripon, P. *et al.* Infection of a human hepatoma cell line by hepatitis B virus. *Proc Natl Acad Sci U S A* **99**, 15655-15660, doi:10.1073/pnas.232137699 (2002).

33 Schulze, A., Mills, K., Weiss, T. S. & Urban, S. Hepatocyte polarization is essential for the productive entry of the hepatitis B virus. *Hepatology* **55**, 373-383, doi:10.1002/hep.24707 (2012).

34 Schneider, C. A., Rasband, W. S. & Eliceiri, K. W. NIH Image to ImageJ: 25 years of image analysis. *Nat Methods* **9**, 671-675 (2012).

35 Berg, S. *et al.* ilastik: interactive machine learning for (bio)image analysis. *Nat Methods* **16**, 1226-1232, doi:10.1038/s41592-019-0582-9 (2019).

36 Zehnder, B., Urban, S. & Tu, T. A Sensitive and Specific PCR-based Assay to Quantify Hepatitis B Virus Covalently Closed Circular (ccc) DNA while Preserving Cellular DNA. *Bio-protocol* **11**, e3986, doi:10.21769/BioProtoc.3986 (2021).

Figures

Figure 1

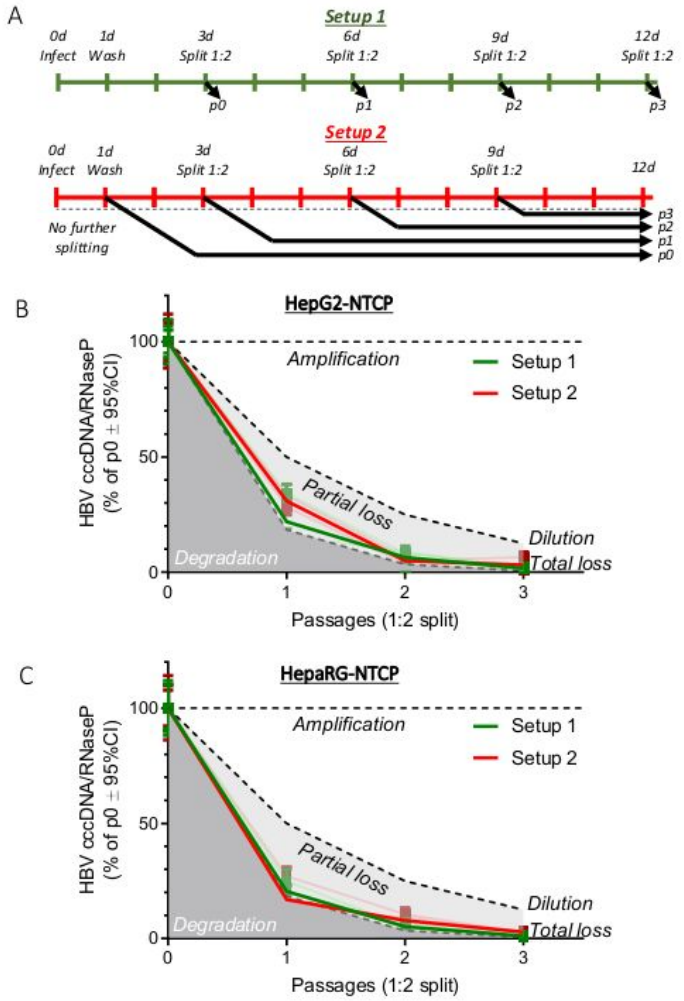

Figure 1. cccDNA levels are profoundly reduced after rounds of cell mitosis in HepG2-NTCP and HepaRG-NTCP cells.

(A) Two experimental setups were used to study the fate of cccDNA following cell mitosis with the main difference being whether cells left over from the splitting were immediately lysed (Setup 1, green) or cultured until 12dpi before DNA was extracted and analysed by cinqPCR (Setup 2, red).

(B and C) Dilution and complete loss models (top and bottom dashed lines, respectively) predict different levels of cccDNA decrease (50 and 18.4% of the pre-split value per passage, respectively). The area between these two models (light grey) represents a model where there is partial loss of cccDNA during mitosis. Levels higher than the dilution model would suggest that cccDNA is somehow amplified following mitosis (amplification, white area), whereas levels lower than the loss model (degradation, dark grey area) would suggest other cccDNA degradation mechanisms, e.g. cytokine-induced cccDNA degradation. HepG2-NTCP (top) and HepaRG-NTCP (bottom) cells were infected and harvested as per setup 1 or 2. The cccDNA decrease according to the dilution and loss models (dashed lines) were predicted using only the 0 passage (p0) time-point. Data points (connected by light lines) represent 3 independent experiments and the mean observed values for setup 1 or setup 2 are shown in solid green and red lines, respectively.

Figure 1

See image above for figure legend

Figure 2

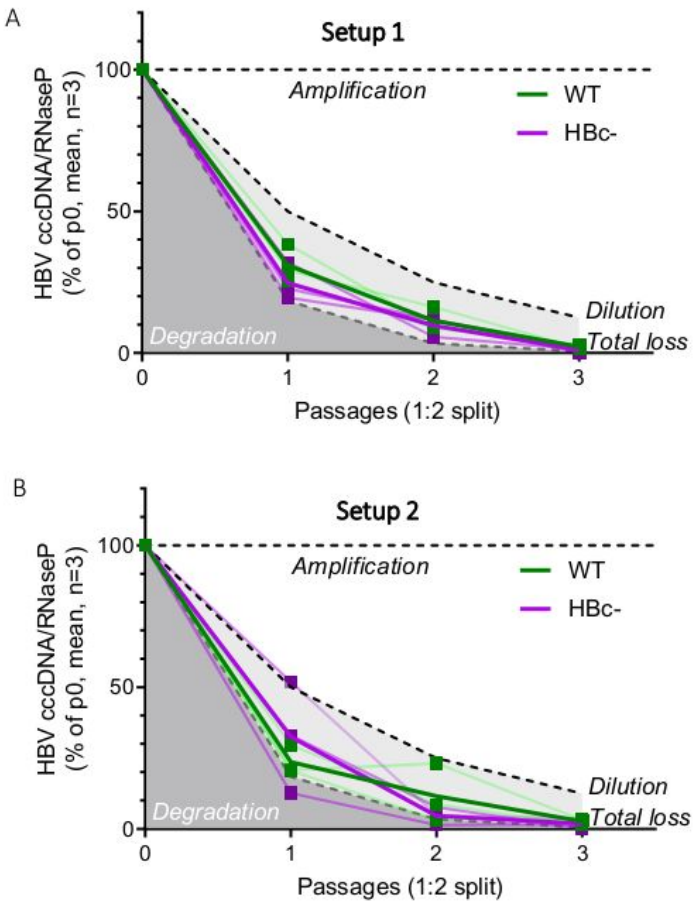

Figure 2. Mitosis-associated cccDNA loss is unaffected by *de novo* viral replication.
HepG2-NTCP cells were infected with either wild-type HBV (green) or replication-deficient HBV mutants containing a stop-codon in the HBc ORF (purple). The infected cells were then serially split according to Setup 1 (A) or Setup 2 (B), as described in Figure 1A. Data points (connected by light lines) represent 3 independent experiments and the mean observed values are shown in solid green and purple lines for WT and HBc-deficient mutant-infected cells, respectively.

Figure 2

See image above for figure legend

Figure 3

See image above for figure legend

Figure 4

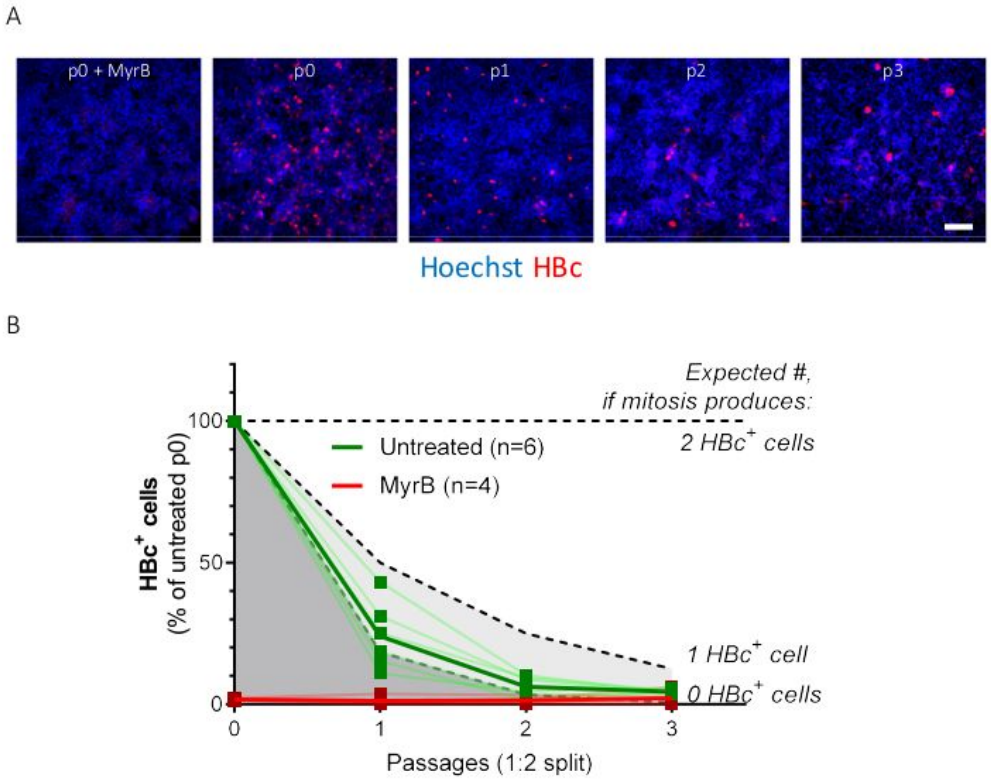

Figure 4. Number of HBc-positive cells decrease with serial passaging consistent with cccDNA loss with mitosis.

(A) HBV-infected HepG2-NTCP cells were treated as per setup 2 (Figure 1A), fixed at 12 days post-infection, and visualised by fluorescence microscopy (HBc in red, Hoechst staining for cell nuclei in blue). Scale bar = 100 µm. MyrB = cells pre-treated with HBV entry inhibitor Myrcludex B as a negative control. (B) A marked decrease in HBc-positive cells was observed with each additional split (green), highly consistent with the loss of HBV cccDNA in daughter cells of infected hepatocytes. Dashed lines represent the number of cells expected per split if 1 or 2 daughter cells (dilution model) or 0 daughter cells (complete loss model) were HBc-positive following mitosis. The percentage of HBc-positive cells was calculated by dividing the number of HBc-positive cells by the number of nuclei in 5 randomly-picked fields of view. Few RFP-positive cells were observed in those pre-treated with the HBV entry inhibitor Myrcludex B (red), showing *bona fide* infection had occurred.

Figure 4

See image above for figure legend

Figure 5

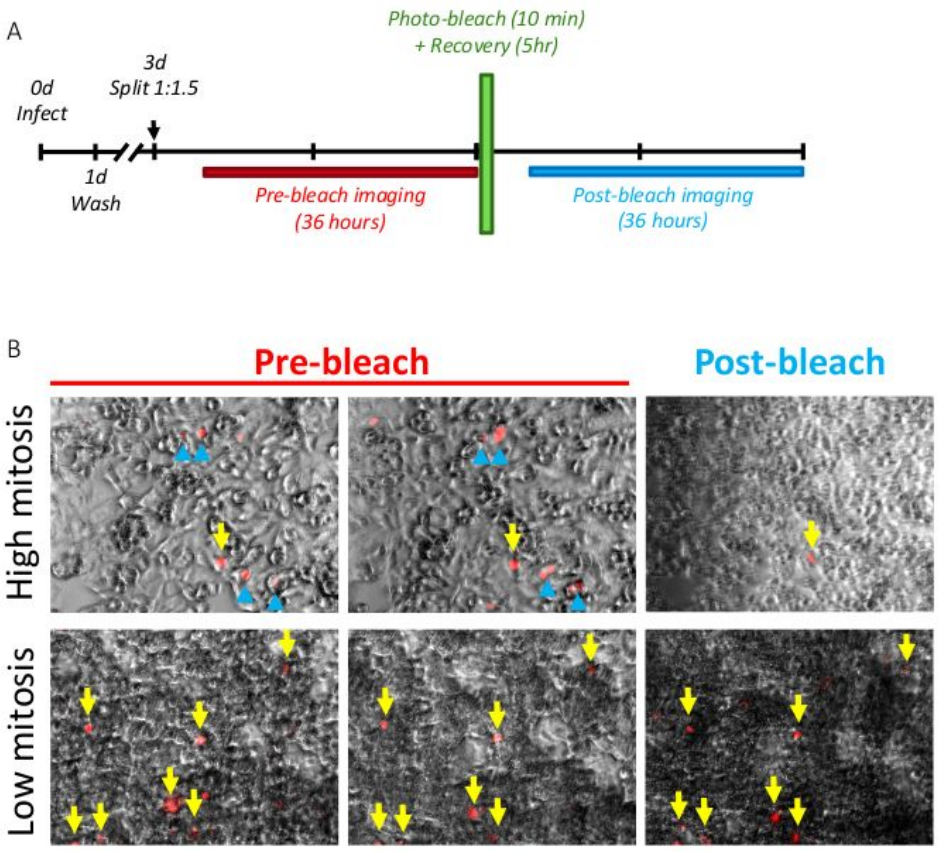

Figure 5. Live-cell imaging shows that HBV-infected cells that undergo mitosis produce viable daughter cells free of transcriptionally active cccDNA.

(A) HepG2-NTCP cells infected with a tRFP-expressing reporter HBV and reseeded at a lower density (equivalent to a 1:1.5 split) in a chamber-slide. After allowed to reattach to the slide bottom for 12 hours, the cells were live-imaged in a humidity-, heat- and CO_2-controlled chamber (1 capture every 15 minutes for 36 hours). Cells were then photo-bleached with 10 minutes exposure of 560/40nm laser light and cells were allowed to recover for 5 hours to limit excess photo-toxicity associated with image acquisition. Live acquisition was then continued for another 36 hours in the post-bleaching stage. Acquisition was measured at 40x with excitation filters at 560/40nm and emission filters at 630/75nm for RFP fluorescence and white light for phase contrast.

(B) Stills from live imaging in pre-bleach (left and centre panels) and post-bleach (right panel) time-points in fields of view with low confluence (high mitosis, top row) or high confluence (low mitosis, bottom row). RFP-positive cells that did not undergo mitosis in the pre-bleach period are marked with a yellow arrow, while cells in which mitosis was observed are marked with a blue triangle. No RFP-positive cells that underwent mitosis maintained positive staining after bleaching.

Figure 5

See image above for figure legend

Supplementary Files

This is a list of supplementary files associated with this preprint. Click to download.

- figureS1.jpg